CRACK GROWTH RESPONSE OF ALLOY 690 IN SIMULATED PWR PRIMARY WATER

M. B. Toloczko and S. M. Bruemmer
Pacific Northwest National Laboratory, P.O. Box 999, Richland, WA 99352

Abstract

The stress corrosion crack growth response of three extruded alloy 690 CRDM tube heats was investigated in several thermomechanical conditions. Extremely low propagation rates (<1x10^{-9} mm/s) were observed under constant stress intensity factor (K) loading at 325-350°C in the as-received, thermally treated (TT) materials despite using a variety of transitioning techniques. Post-test observation of the crack-growth surfaces revealed only isolated intergranular (IG) cracking. One-dimensional cold rolling to 17% reduction and testing in the S-L orientation did not promote enhanced stress corrosion rates. However, somewhat higher propagation rates were observed in a 30% cold-rolled alloy 690TT specimen tested in the T-L orientation. Cracking of the cold-rolled material was promoted on grain boundaries oriented parallel to the rolling plane with the % IG increasing with the amount of cold rolling.

I. INTRODUCTION

Alloy 690 is now used for many light-water reactor applications to replace more stress-corrosion cracking (SCC) susceptible alloy 600. An important example has been for pressurized water reactor (PWR) vessel penetrations such as control-rod-drive mechanism (CRDM) nozzles. This higher Cr alloy has been found under most circumstances to be highly resistant to SCC initiation and propagation. In most cases [1-5], tests on alloy 690 in PWR primary water have not shown any cracking. However, very high propagation rates have recently been reported [5-8] for alloy 690 plate materials after one-dimensional (1D) rolling or tensile straining. Crack-growth-rate test results are described in this paper to expand on these observations. Representative alloy 690 CRDM tube heats are evaluated both in the as-received condition and after selected thermomechanical treatments.

II. EXPERIMENTAL

Materials used for the study were taken from three different heats of alloy 690 CRDM tubing provided by Valinox Nucléaire in the as-received, thermally treated (TT) condition. As shown in Table 1, the compositions of the different heats are nearly identical. Four different pieces of tubing were used to make 0.5T compact tension (CT) specimens for crack growth testing. For the RE243 heat, specimens were taken from two different tubes, with one tube having a larger diameter allowing the cold-rolled (CR) material to be machined for testing in the S-L orientation.

The three different CRDM heats exhibited similar microstructures with uniform, equiaxed grain sizes (~100 μm in diameter) across the wall thickness except at the outer 10 mm where the grain size was found to drop by about 50%. As a means to examine the effects of variations in microstructure, barstock was cut from the RE243 heat tubing and given several different thermal or thermomechanical treatments. A carbide-modified (CM) condition was obtained by annealing the as-received material at 1100°C for 1 h followed by a water quench. This treatment reduced the carbide density and increased carbide size on most boundaries while maintaining nearly the same average grain size as the TT material. Some pieces of the CM and TT materials were then 1D rolled at room temperature to a 17% reduction in 2 passes or a 30% reduction in 6 passes. Because of the tubing wall thickness, the maximum reduction possible for an S-L oriented specimen was 17% and the 30% CR material was tested in the T-L orientation. Hardness measurements across selected CT samples indicated a lower hardness near the midplane for the 17% CR samples, but uniform hardness across the 30% CR samples. Consistent with the higher directional damage, grains were noticeably elongated along the rolling plane in the 30% CR specimen but no obvious change was identified for the 17% CR specimen. The complete matrix of conditions examined is shown in Table 2.

Table 1. Composition of the Alloy 690 CRDM Heats

Heat Tube ID	Composition, wt%
RE243 Tube 2216 and 2360	Ni-28.9Cr-10.4Fe-0.02C-0.3Mn-0.35Si-0.14Al-0.23Ti-0.024N-0.0005S-0.008P
WP140 Tube 2502	Ni-29.0Cr-10.4Fe-0.03C-0.3Mn-0.33Si-0.18Al-0.3Ti, <0.001S
WP142 Tube 2541	Ni-29.0Cr-10.5Fe-0.02C-0.3Mn-0.35Si-0.18Al-0.27Ti-0.037N-0.0006S-0.006P

Table 2. Alloy 690 CRDM Materials

Spec. #	Heat - Tube	Material Condition
CT014	RE243 - 2360	As-received TT
CT015	RE243 - 2360	CM (1100C/1 h/WQ)
CT019	RE243 - 2360	CM + 17% CR S-L
CT020	RE243 - 2360	TT + 17% CR S-L
CT022	RE243 - 2216	TT + 30% CR T-L
CT023	RE243 - 2216	CM + 30% CR T-L
CT026	WP142 - 2541	As-received TT
CT027	WP140 - 2502	As-received TT

Side grooves of 5% were used on the 0.5T CT specimens for all the tests. Specimens were cut in the C-L orientation relative to the tubing. Barstock was oriented so that the desired orientation of the specimens relative to the rolling plane could be achieved while maintaining the C-L orientation relative to the tubing. The orientation of the specimens obtained from the CR materials is shown in Figure 1. Specimens were taken from material that was at least 10 mm away from the tube OD.

Crack-growth testing was performed in recirculating water autoclave systems capable of operation up to 360°C. Flow rate through the four-liter autoclave is maintained at 200 cc/min giving ~3.5 autoclave water exchanges per hour. Water chemistry is maintained through a combination of a boric acid and lithium hydroxide saturated mixed bed resin demineralizer, active stock solution injection, and a continuously circulating four-liter water column used to bubble gasses through the autoclave feedwater. Active load control is obtained through the use of software that interacts with a load cell and a servoelectric load frame. Crack length is estimated in-situ using a reversing direct current potential drop (DCPD) system. Intrinsic resistivity change of the test material at PWR water temperature is handled by DCPD reference potentials attached directly to the test specimen. DCPD noise in our systems causes a data scatter of approximately ±1 µm enabling crack growth rates as low as $5x10^{-10}$ mm/s to be indicated during long-term exposures. For several tests, a Cu/Cu_2O zirconia membrane reference electrode was utilized to allow measurement of the corrosion potential of the specimens. Crack growth tests were performed with two specimens in series allowing a greater range of material conditions to be examined in a shorter period of time. Testing was primarily performed in 325°C or 350°C simulated PWR primary water (2000 ppm B and 2 ppm Li) with a dissolved hydrogen content of 29 cc/kg H_2. The standard K value used for testing was 30 MPa√m and was controlled on one of the two specimens in series. Some specimens were tested at 40 MPa√m as well and will be noted in the results.

Specimens were first pre-cracked in air followed by extending the precrack by cycling in the high-temperature water environment. A variety of loading conditions were used to transition the transgranular (TG) crack front to an intergranular (IG) SCC crack. The general approach was to transition by going to slower and slower crack tip strain rates, typically by reducing the cycling frequency. A range of R values (0.5-0.7) with either a symmetric or a sawtooth (e.g., rapid unload and slow reload) waveform were used followed by the addition of a hold time (1-24 h) separating the periodic unload. No one loading condition was found to promote SCC better than the others, but the general philosophy was to choose "gentle" cycling and cycle + hold condition that moves the crack forward fast enough to encounter as many grain boundaries as possible while still enabling IG propagation if that is a favored path. For these alloy 690 tests, the final transitioning step before establishing constant K was often 0.001 Hz, R=0.5 and hold time of 2.5 h. If propagation rates during these final transitioning steps indicated limited SCC engagement across the crack front, alternative cycling and cycle + hold steps were sometimes applied before going to constant K. In many instances, long-term exposure to gentle cycle + hold and constant K conditions would be evaluated to help confirm the extremely low crack-growth rates.

As part of the general research being conducted on these materials, crack-growth-rate response was also evaluated on some specimens at 50°C in the simulated PWR primary water environment. Earlier [9] tests on alloy 152 weld metal revealed extensive IG cracking during cycling at 50°C. Based on this result and initial alloy 690 tests reported here, the attempt was made to generate a more IG crack front at 50°C for subsequent SCC testing at 350°C.

III. RESULTS AND DISCUSSION

III.A. Crack Growth Response of the Non-Cold Rolled Material

A total of four specimens were tested, two from the RE243 heat, and one each from the WP140 and WP142 heats. An overall plot of the crack growth for the heat RE243 specimens is shown in Figure 2. Very similar behavior can be seen for the TT and CM specimens over the year-long experiment. The first transitioning sequence spent a very long time under "gentle" cycle + hold conditions before going to constant K as shown in Figure 3. It was hoped that IGSCC would be promoted during these conditions, however crack growth rates decreased with time for

both the 2.5 and 24 h hold conditions indicating a lack of engagement. Although there was no sign of an accelerated crack growth rate, constant K was established at ~5200 h and extremely small crack extensions (1-2 μm) were measured by DCPD over the next 1000 h. Since this extension does not represent a meaningful propagation distance, the crack growth rates are simply assumed to be $<5x10^{-10}$ mm/s. The crack fronts were then moved forward into different microstructural regions by cycling and a second transitioning sequence was initiated. Crack-growth response was nearly identical during cycle + hold conditions to that in the first sequence, and it was decided to increase the K level to 40 MPa√m under gentle cycling at 0.001 Hz. As noted in Figure 2, a large jump in crack length was observed likely due to the breaking of ligaments in the wake of the crack front. No discernable increase in constant K, crack-growth rates were found at 40 MPa√m and rates were estimated to be $<5x10^{-10}$ mm/s.

The high-temperature portion of the test was ended and the temperature was decreased to first 100°C and then to 50°C. No indication of crack extension was detected under constant K, so cyclic loading was applied as documented in Figure 4. The crack growth rates at 50°C were similar to that observed during testing at 325°C, however somewhat higher rates were noted for the TT specimen.

Post-test examination of the 325°C crack-growth surfaces revealed predominately TG features for both the TT and CM specimens as illustrated in Figure 5. Only a few isolated IG facets could be identified near final high-temperature crack front and were most likely produced during the cycle + hold and constant K steps at 1500-6500 h. More significant IG cracking was found in the 50°C crack-growth surface for the TT specimen (5a), while the CM specimen remained TG (5b). The higher fraction of IG cracking (~15%) in the TT material was consistent with the higher propagation rates measured during cycling at 50°C.

Heat-to-heat response was evaluated in the next test on alloy 690 CRDM heats WP140 and WP142 both in the as-received, TT condition. Once again, the test was conducted under simulated PWR primary water but at a slightly higher temperature of 350°C Four transitioning sequences were performed to improve SCC engagement as shown in the overview of the entire test in Figure 6. The first three transitioning attempts done at 350°C resulted in very low constant K crack-growth rates. Although these may be slightly higher than seen for the alloy 690 heat RE243 specimens, they remain below $1x10^{-9}$ mm/s. For each attempt, somewhat different cycling and periodic unloading parameters were used during transitioning to constant K conditions. An example of the low-growth rates at constant K is presented in Figure 7. DCPD-measured crack extension is only ~1.5 μm over a period of 600 h.

Crack transitioning at 50°C was used in the last attempt to generate an IG crack front. Based on the IG cracking produced during 50°C cycling in the previous test on the TT material, it was decided to use this approach to generate a more IG crack front for subsequent SCC evaluation at 350°C. Cycling was performed at 50°C over a period of ~650 h using a load ratio of 0.5 with a progressive reduction in frequency to 0.001 Hz for the final step. Loading was then changed to constant K and the temperature increased back to 350°C. The specimen was allowed to sit for ~24 h at 350°C before resuming DCPD crack length measurements. Initial crack-growth rates exceeded $1x10^{-8}$ mm/s as shown in Figure 8, but slowly decreased to $\sim3x10^{-9}$ mm/s over the next 500 h. A variety of reasons for the slowly dropping rate were considered, and among the possibilities was that ligaments or bridges were being left in the wake of the advancing crack. To explore this possibility, a periodic unload was added every 2.5 h at 6750 h. An immediate ~30 μm increase in DCPD-measured crack length was observed at the onset of cycling followed by rates stabilizing at $\sim2x10^{-8}$ mm/s during this cycle + hold loading (similar to that recorded earlier in the test). At this point it was decided to end the test and examine the crack-growth surfaces for evidence of IGSCC.

After air fatigue fracturing the specimens, the specimens were heat tinted at 630°C and ultrasonically cleaned. The resulting tinted crack-growth surface of the WP140 specimen is shown in Figure 9. Five regions were identified through surface tint and transition lines on the surface, and then matched to DCPD measurements of crack length. Starting from the crack notch, the first region with the darkest blue tint is the air fatigue pre-cracking surface. The next three regions are crack growth during gentle cycling and constant K conditions at 350°C. The final region with a mix of blue and gold tint represents ~0.5 mm of crack growth at 50 and 350°C. SEM of the crack growth surface (Figure 10) revealed nearly 100% TG crack growth everywhere except for the final 50/350°C region where ~50% of the surface is IG. At this time, it is not clear what portion of this region represents constant K IGSCC propagation at 350°C. Neither optical nor SEM observations show the presence of a final band that might be expected based on the ~90 μm extension on the crack growth plot. The high initial crack growth rate at this last step at 350°C suggests that this initial response may have been due to oxide formation in cracks influencing the DCPD measurement [~~8~~9]. The hydrogen concentration of

20 cc/kg produces an electrochemical potential well into the region of Ni metal stability at 50°C, while it is near the Ni/NiO stability line at 350°C. It is thought that the actual crack growth rate during the majority of this final step at 350°C was near the final observed rate of ~$3x10^{-9}$ mm/s. Additional experiments are being performed to investigate the effect of this temperature and electrochemistry change on the DCPD measurement of crack length.

III.B. Crack Growth Response of 1D CR Material

The crack growth response of alloy 690, heat RE243 specimens was evaluated after 1D cold rolling to 17% in the S-L orientation and to 30% in the T-L orientation. An overview of results for the 17% CR S-L materials tested in 325°C water is presented in Figure 11. Several measurements of constant K crack growth rate were made, and all were at or below $1x10^{-9}$ mm/s. A higher resolution crack growth plot showing this steady, but extremely slow propagation at constant K is shown in Figure 12. After several attempts to promote higher growth rates using different transitioning steps that were found to give similar results under PWR primary water conditions, H_2 injection was stopped and replaced with 2400 ppb O_2 plus 45 ppb sulfate. While the oxidizing environment did increase propagation rates by ~3X, they remained very low under constant K. PWR primary water conditions were re-established for the final part of the test and K was slowly increased to 40 MPa√m via a dK/da technique. DCPD-measured crack length showed that the higher K promoted slightly increased growth rates during cycle + hold loading, but did not appear to promote SCC at constant K. In comparing the overall response of the two material conditions, the CM specimen exhibited higher growth rates during cycling than the TT specimen but both showed similar low growth at constant K.

Post-test optical images of the crack-growth surfaces are shown in Figure 13. The greater amount of crack extension measured by DCPD in the CM specimen is confirmed by these images showing the CM specimen to have cracked ~0.5 mm further than the TT specimen. For both specimens, three distinct regions of crack growth after the precracking phase are apparent with the regions corresponding to the three different phases of the test. The more reflective surface of the CM specimen suggests the possibility of IG cracking, and this was confirmed by SEM observations as shown in Figure 14(a). These regions have ~15% IG features and correspond to phases of the test where cycle + hold or constant K loading was performed. The TT specimen exhibited primary TG cracking with only isolated IG facets as illustrated in Figure 14(b).

It is interesting to note that IG cracking was increased in the 17% S-L specimens over the non-CR specimens, but the amount of IG cracking was still low compared to tests on 1D CR S-L alloy 690 plate by others. Several possible reasons exist for the lack of extensive IGSCC in these 1D CR S-L alloy 690 CRDM materials. One possibility is that the extruded CRDM tubing microstructures are more resistant to the 1D damage than other alloy 690 materials that show very high SCC crack growth rates after cold rolling. It is also possible that there may have been insufficient cold work in the crack-growth plane to accelerate SCC. Although the total reduction for the CRDM tube material was 17%, the amount of cold work in the center of the sample where propagation occurred was somewhat less than the total reduction. Additional work is needed to determine the response of these CRDM materials to higher levels of 1D S-L deformation.

A T-L orientation was used to examine a higher level of 1D cold rolling in these CRDM tubes using 0.5T CT specimens. An overview of the crack growth response of the 30% CR T-L specimens is shown in Figure 15. As with 17% CR S-L specimens, several transitioning sequences were performed leading to three observations of constant K crack-growth response. The first instance of constant K at ~1500 h produced propagation rates that were higher than the 17% CR S-L material, but decreasing with time. After additional cycle + hold steps were applied, the TT and CM specimens exhibited steady crack-growth rates of $1.0x10^{-8}$ and $1.0x10^{-9}$ mm/s, respectively, as shown in Figure 16. With the higher observed rate in the TT specimen, the test was allowed to continue at constant K for 1000 h producing a crack extension of ~40 μm in the TT specimen. As a final step, K was increased to 40 MPa√m by dK/da and transitioned back to constant K where a mild enhancement of SCC was again indicated in the TT specimen.

Figure 17 shows optical images of the crack-growth surface for the 30% CR T-L specimens. The three phases of the test are not easily resolved probably due to the shorter amount of crack extension between primary transitioning attempts and the less aggressive transitioning steps employed. The most striking difference between the specimens is that the CM specimen has a relatively flat crack front across the width, while the TT specimen has an uneven crack front with a large number of fingers. SEM images (Figure 18) reveal that IG cracking occurred at the crack front for both specimens with a much higher fraction of IG facets for the TT specimen. For both materials, nearly all cracked

grain boundaries were oriented approximately parallel to the rolling plane and would have sustained the most damage from the cold-rolling operation. Despite the less favorable orientation relative to the crack-growth plane, IG cracking was promoted on many of these boundaries. The different IG growth between the TT and CM specimens suggests that minor modification in the grain boundary carbide size and density may influence rolling-induced damage and SCC response. If this 30% CR alloy 690TT material could have been tested in the S-L orientation, crack-growth rates would have likely been much higher.

IV. Summary and Conclusions

Representative alloy 690 CRDM plant materials were studied to investigate the SCC crack-growth response in the as-received TT and several modified conditions. A variety of different transitioning methods were employed in an attempt to promote SCC engagement and effectively measure propagation rates under constant K conditions. None of the transitioning methods were found to produce significant IG cracking in PWR primary water at 325 or 350°C for the non-CR materials. Crack-growth response for three different alloy 690 heats in the as-received TT condition, and one heat also in the CM condition, was essentially the same. Steady propagation was observed at constant K, but only at extremely low rates ($\leq 1 \times 10^{-9}$ mm/s) as summarized in Figure 19.

Crack-growth-rate testing of the 17% CR S-L specimens showed similarly low propagation rates during both cycle + hold and constant K phases. Despite the having rates similar the non-CR materials, SEM observations of the crack-growth surfaces revealed noticeable IG cracking (~15% in the CM specimen). This suggests that the 17% CR condition does influence grain boundary susceptibility to SCC, but the amount of damage was not sufficient to degrade overall SCC resistance even for the S-L orientation. The CM+30% CR T-L specimen had similar resistance to cracking as the 17% CR S-L specimens, but the TT+30% CR specimen showed extensive IG cracking with the constant K crack growth rate reaching as high as 1.2×10^{-8} mm/s. IG cracking in these specimens during 350°C testing was primarily limited to grain boundaries that were parallel to the rolling plane.

Limited testing was also performed at 50°C initially to evaluate the potential for environment-assisted cracking at low temperatures and then later to promote a more IG crack front for subsequent high-temperature SCC testing. Significant IG cracking was found to occur during gentle cycling at 50°C in the as-received alloy 690TT materials consistent with concurrent tests [9] on alloy 152 weld metal under similar conditions. Even with a high degree of IG engagement at crack front created at 50°C, DCPD-measured propagation rates at 350°C decreased rapidly with time and approached the low rates observed previously. Moreover, careful examination of the crack growth surface revealed no clear indication of crack advance after converting from 50°C to 350°C.

These results support the general conclusion that the alloy 690 CRDM materials are extremely resistant to SCC in PWR primary-water environments. While 1D cold rolling promoted some IG cracking in the CRDM tube heats, SCC growth rates remained very low compared to prior tests [5-8, 10] on alloy 690 plate heats as shown in Figure 20. Additional testing is needed on plant-representative alloy 690 materials along with research to determine the root causes for the observed high IGSCC susceptibility after 1D deformation in certain heats.

Acknowledgements

This research was supported by the Office of Nuclear Regulatory Research, U.S. Nuclear Regulatory Commission (NRC) under Contract DE-AC06-76RLO 1830. Pacific Northwest National Laboratory (PNNL) is operated for the U.S. Department of Energy by Battelle Memorial Institute. Technical assistance of Rob Seffens, Clyde Chamberlin and Ruby Ermi at PNNL are recognized along with helpful discussions with Darrell Dunn and Carol Moyer of the NRC. Continuing important interactions are also acknowledged with Peter Andresen of General Electric Global Research.

References

1. K. Smith, A. Klein, P. Saint-Paul and J. Blanchet, "Inconel 690 A Material with Improved Corrosion Resistance for PWR Steam Generator Tubes," *Proc. 2nd Int. Symp. Environmental Degradation of Materials in Nuclear Power Systems – Water Reactors,* Monterey, CA, American Nuclear Society, 1986, p. 319.
2. K. Norring, J. Engstrom and H. Tornblom, "Intergranular Stress Corrosion Cracking of Steam Generator Tubing: 25,000 Hours Testing of Alloy 600 and Alloy 690," *Proc. 4th Int. Symp. Environmental Degradation of Materials in Nuclear Power Systems – Water Reactors,* Traverse City, MI, National Association of Corrosion Engineers, 1990, p. 12-1.
3. F. Vaillant, J. D. Mithieux, O. De Bouvier, D, Vanchon, G. Zacharie, Y. Brchet and F. Louchet,

"Influence of Chromium and Microstructure on Creep and PWSCC of Nickel-Base Alloys," *Proc. 9th Int. Conf. Environmental Degradation of Materials in Nuclear Power Systems – Water Reactors,* Newport Beach, CA, NACE International, 1999.

4. J. M. Boursier, F. Vaillant, P. Saulay, Y. Brechet and G. Zacharie, "Effects of the Strain Rate on the Stress Corrosion Cracking in High-Temperature Primary Water: Comparison Between Alloys 690 and 600," *Proc. 12th Int. Conf. Environmental Degradation of Materials in Nuclear Power Systems – Water Reactors,* Stevenson, WA, American Nuclear Society, 2003, p. 199.

5. D. J. Paraventi and W. C. Moshier, "Alloy 690 SCC Growth Rate Testing," *Proc. Workshop on Cold Work in Iron- and Nickel-Base Alloys,* Toronto, Canada, EPRI, June 2007.

6. P. L. Andresen, M. M. Morra, J. Hickling, A. Ahluwalia and J. Wilson, "PWSCC of Alloys 690, 52 and 152," *Proc. 13th Int. Conf. Environmental Degradation of Materials in Nuclear Power Systems – Water Reactors,* Whistler, B. C., Canadian Nuclear Society, 2007.

7. P. L. Andresen, M. M. Morra, J. Hickling, K. Ahluwalia and J. A. Wilson, "Effect of Deformation and Orientation on SCC of Alloy 690," *Proc. 14th Int. Conf. Environmental Degradation of Materials in Nuclear Power Systems – Water Reactors,* Virginia Beach, VA, American Nuclear Society, 2009, these proceedings.

8. B. Alexandreanu, "The Stress Corrosion Cracking Behavior of Alloys 690 and 152 Weld in a PWR Environment," ibid 7, these proceedings.

9. M. B. Toloczko and S. M. Bruemmer, "Crack-Growth Response of Alloy 152 and 52 Weld Metals in Simulated PWR Primary Water," ibid 7, these proceedings.

10. B. Alexandreanu, private communication, 2009.

11. K. Arioka, private communication, 2009.

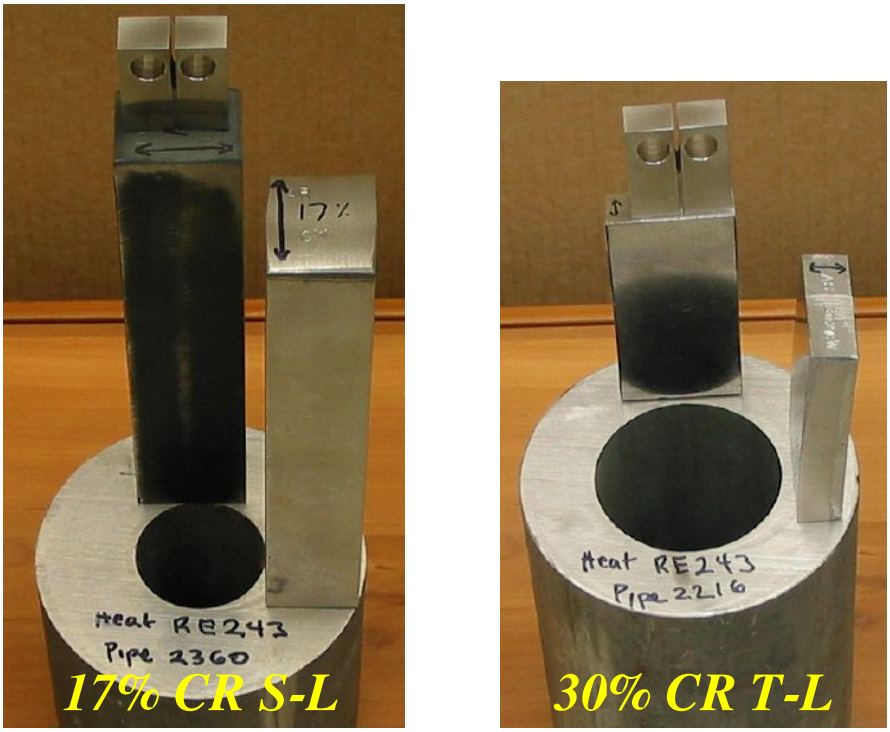

Figure 1. Orientation of the cold-rolled specimens relative to rolling plane and tubing coordinates.

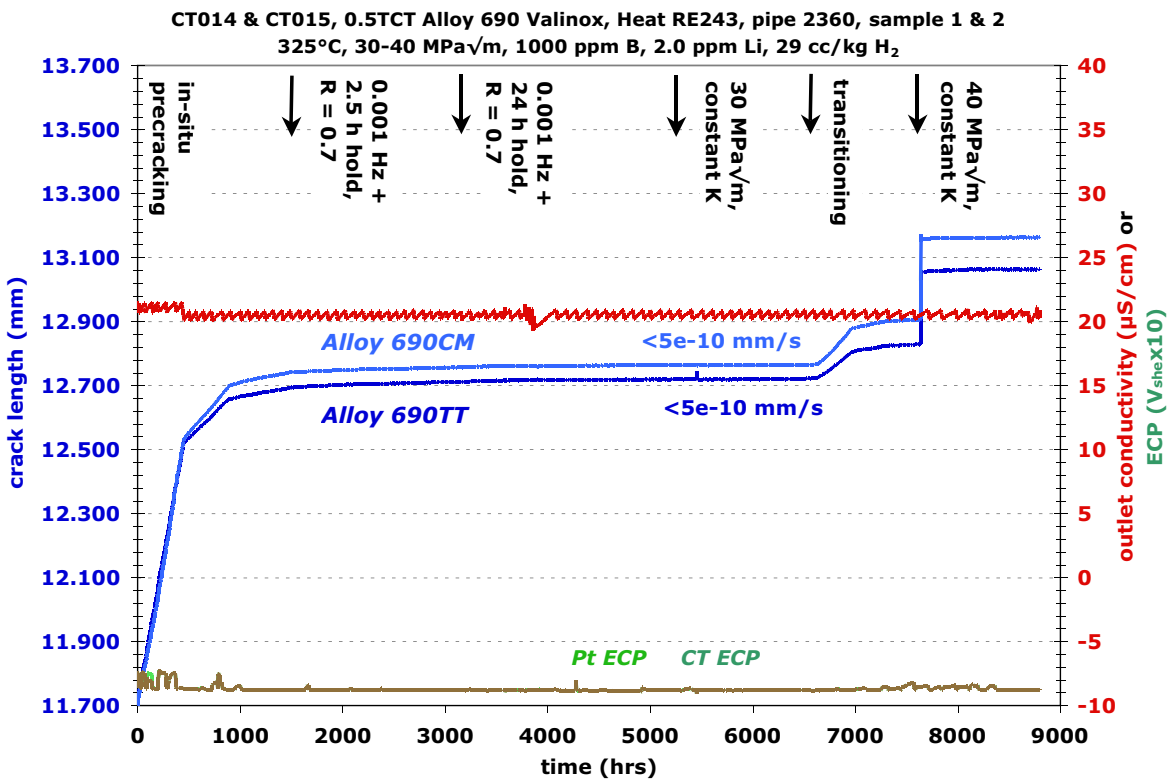

Figure 2. Overall crack-growth response of TT and CM alloy 690 heat RE243 at 325°C.

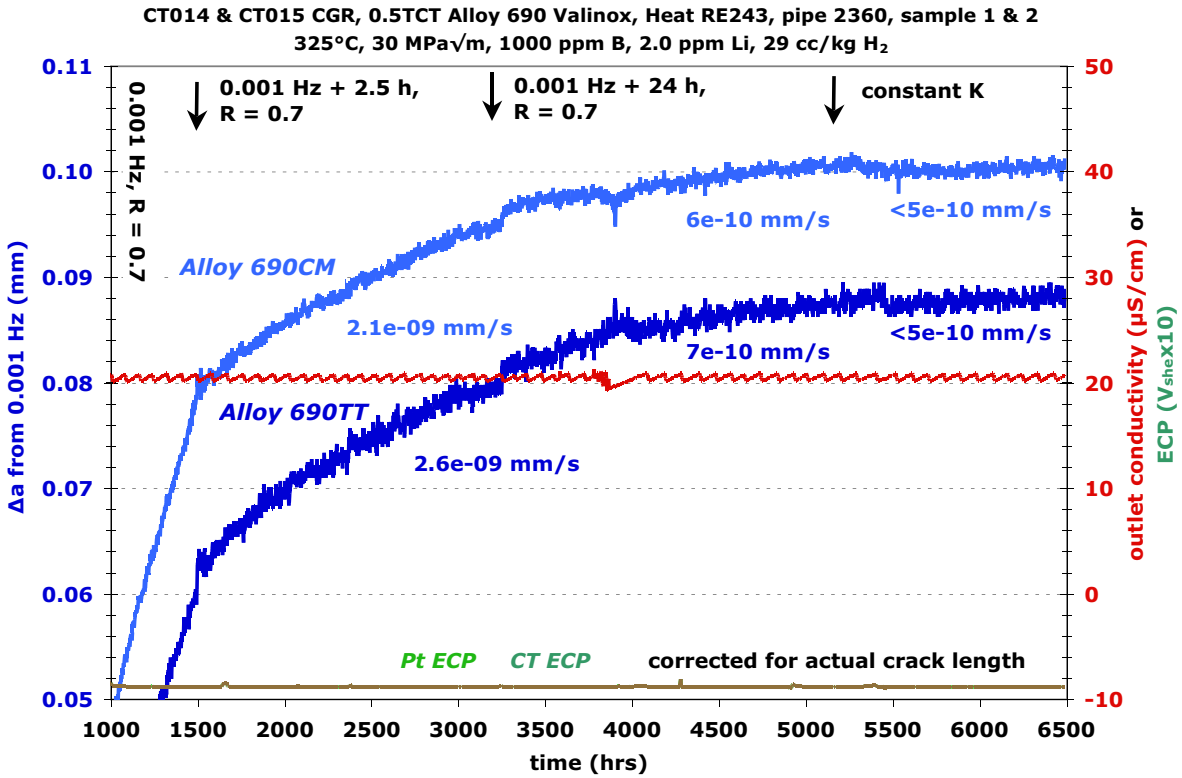

Figure 3. Crack growth response of TT and CM alloy 690 during transitioning to constant K at 325°C.

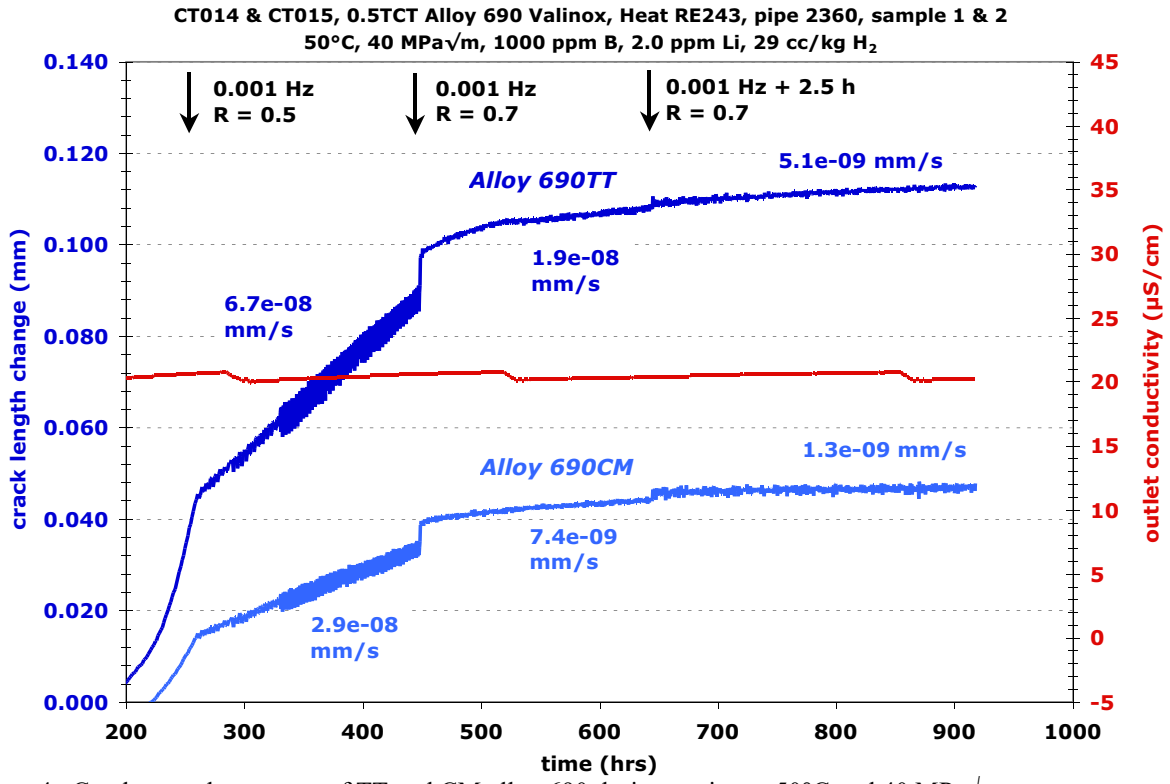

Figure 4. Crack-growth response of TT and CM alloy 690 during testing at 50°C and 40 MPa√m.

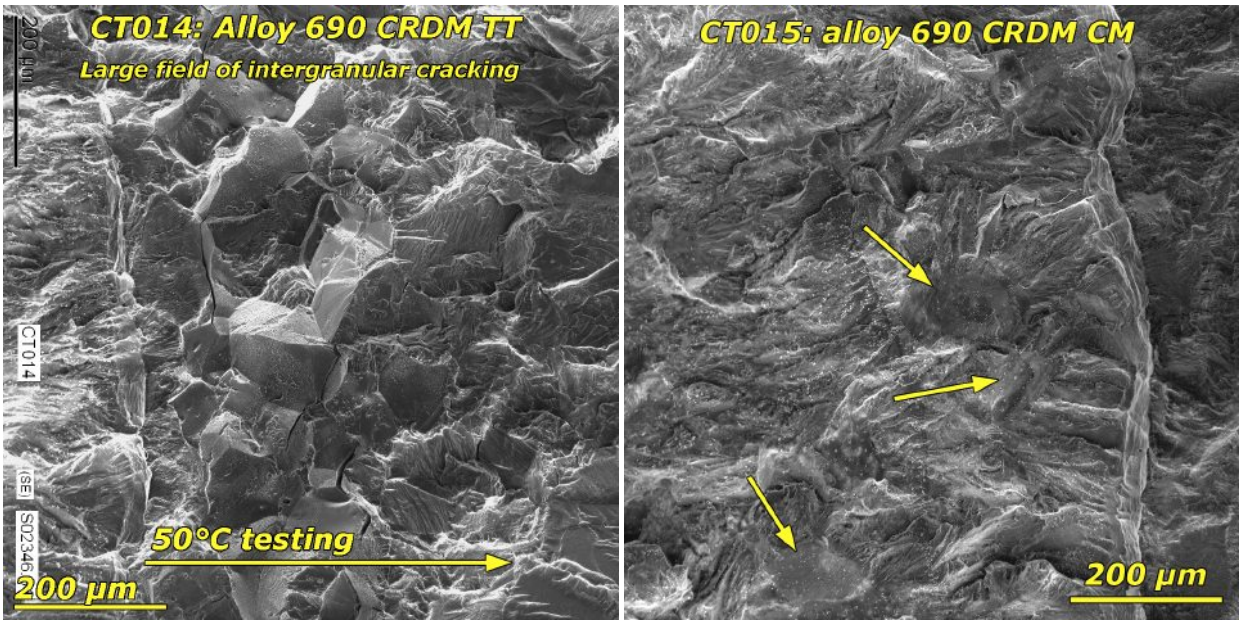

Figure 5. SEM image showing IG cracking for the alloy 690 TT specimen during testing at 50°C (a) and primarily TG cracking for the CM specimen (b) although isolated IG facets are identified.

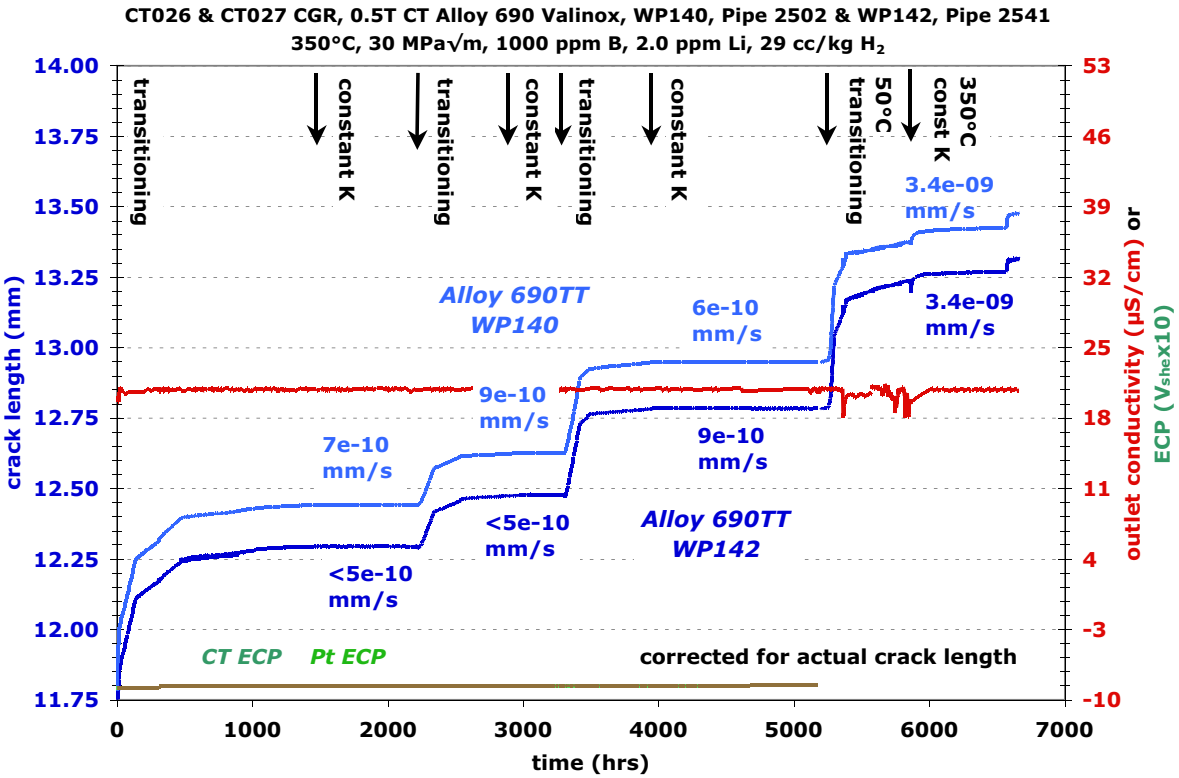

Figure 6. Overview of the crack-growth response for the alloy 690 CRDM heats WP140 and WP142 at 350°C.

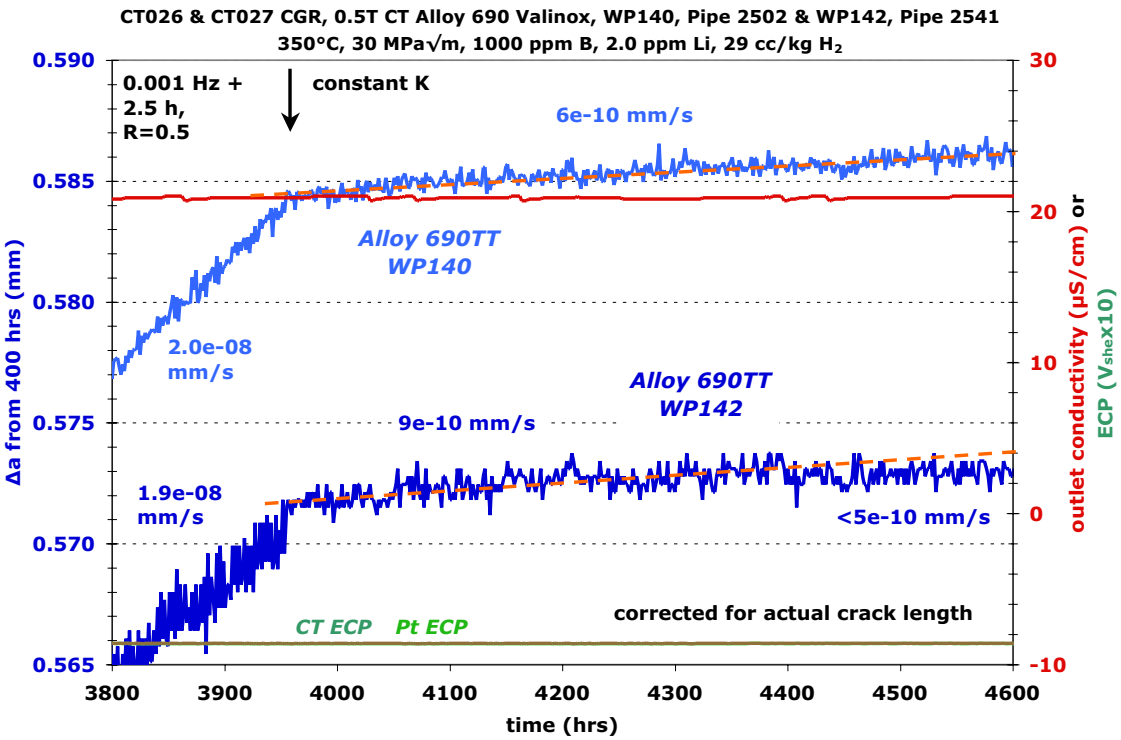

Figure 7. Initial constant K crack-growth response for the alloy 690 CRDM heats WP140 and WP142 at 350°C.

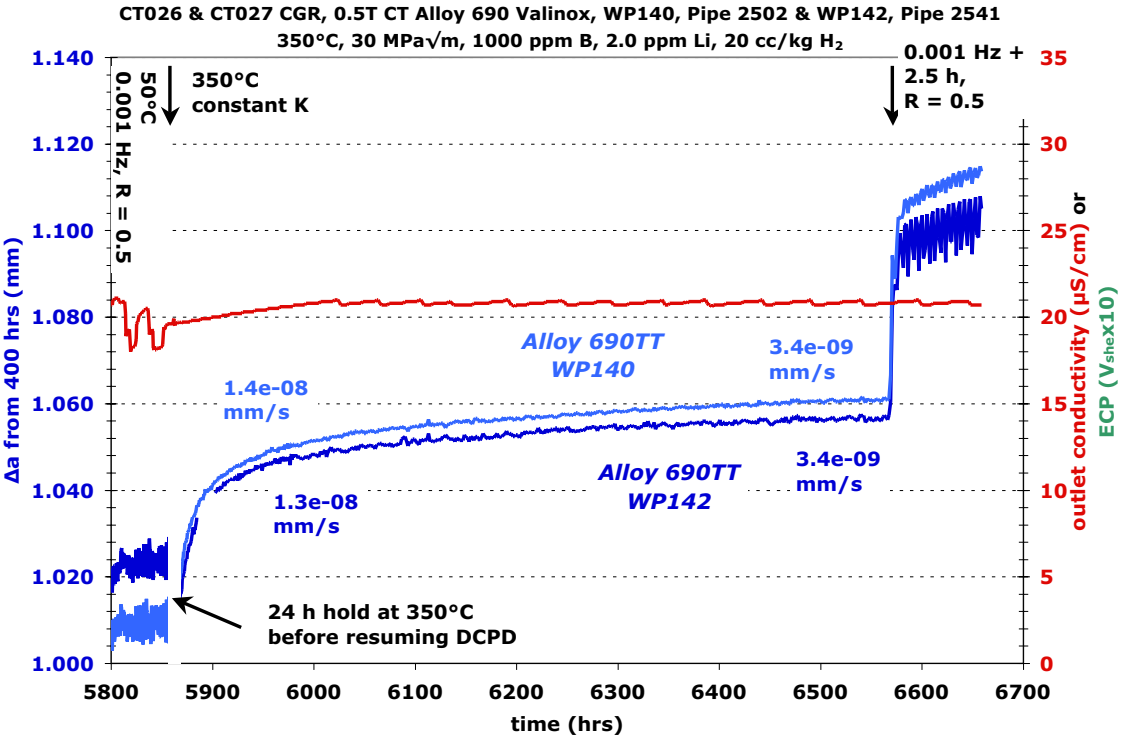

Figure 8. Crack-growth response of alloy 690 heats WP140 and WP142 after crack extension during at 50°C.

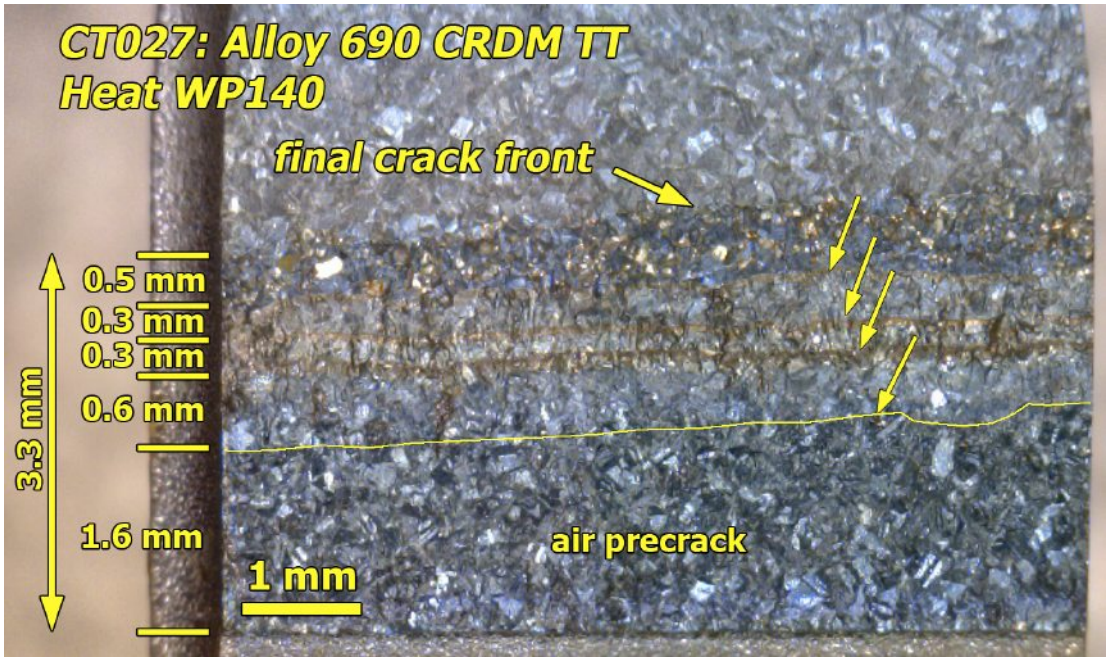

Figure 9. Optical image of the crack-growth surface of the alloy 690 CRDM heat WP140 specimen. Color variation is heat tint due to baking the specimen at 600°C after fatigue fracture in air.

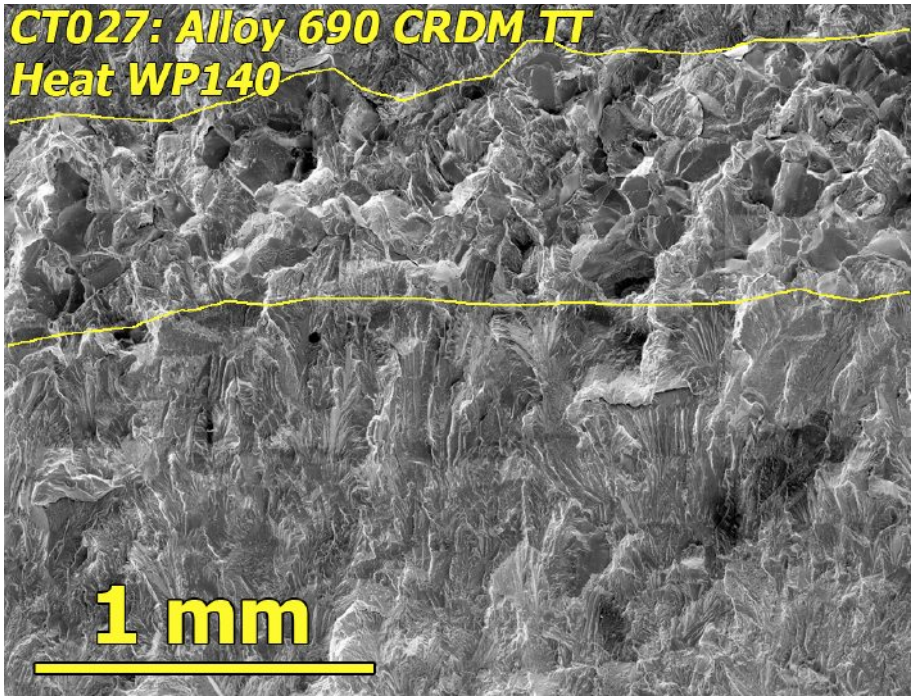

Figure 10. Portion of the crack-growth surface of the heat WP140 specimen. Crack growth in the area between the lines took place during 50°C and the subsequent 350°C phases of the crack growth rate test.

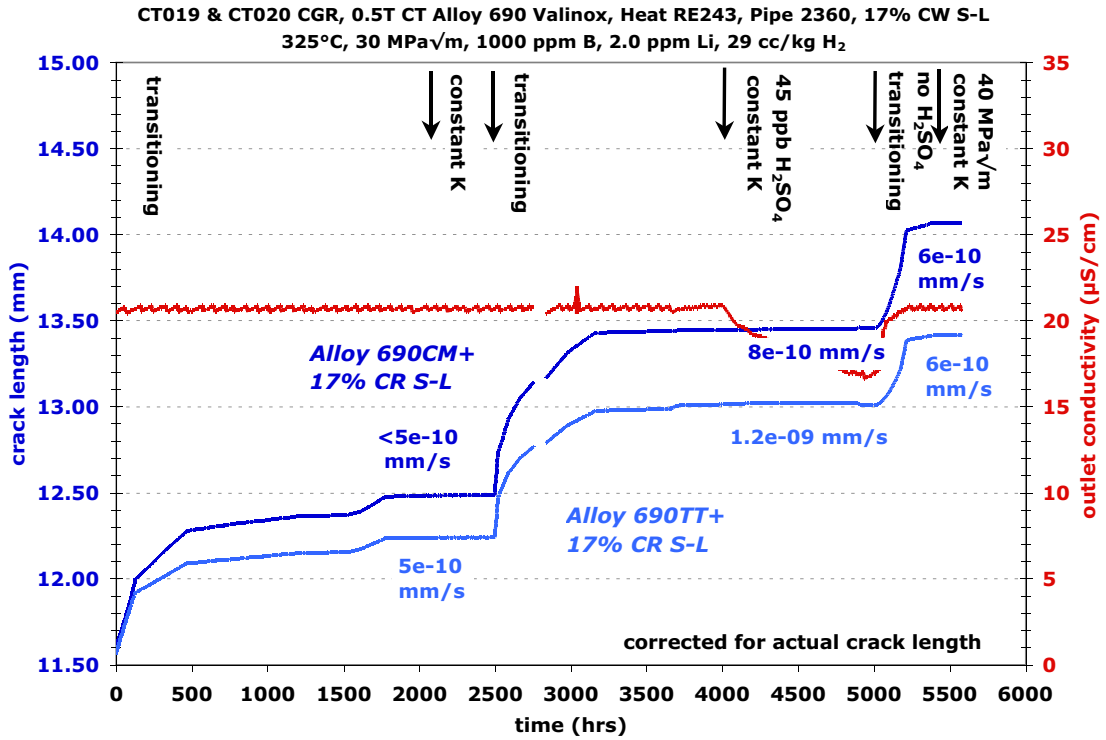

Figure 11. Overview of crack-growth response of the 17% CR S-L specimens tested at 325°C.

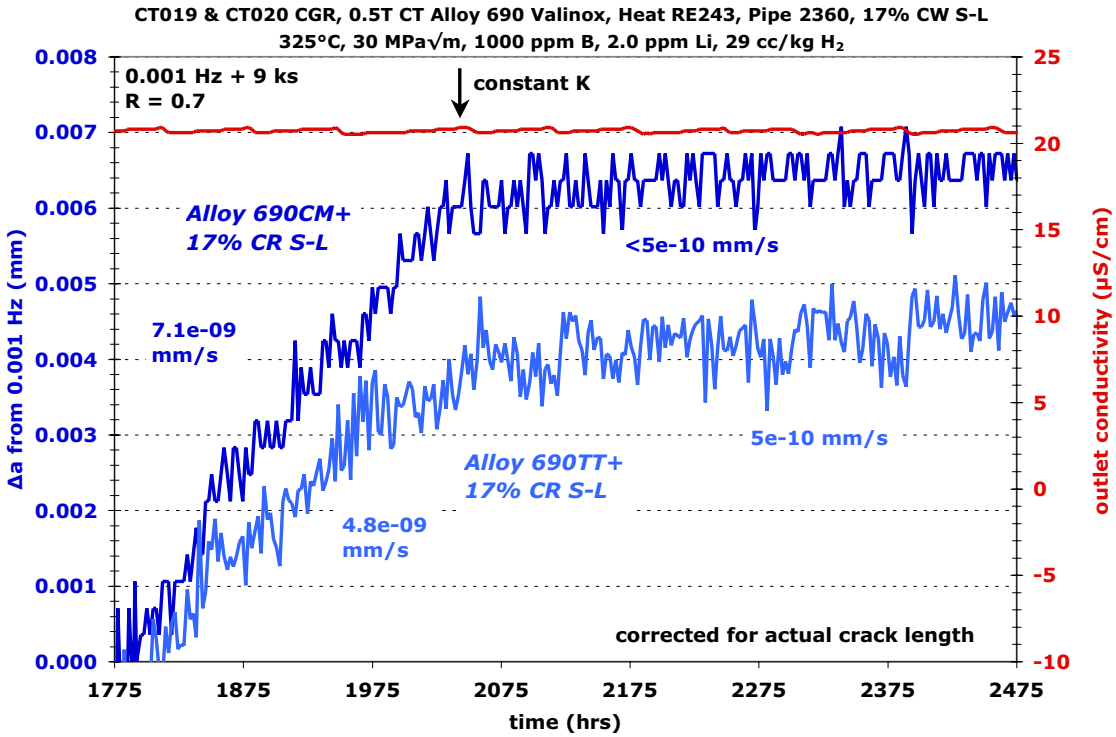

Figure 12. Crack growth response of the 17% CR S-L specimens during first instance of constant K.

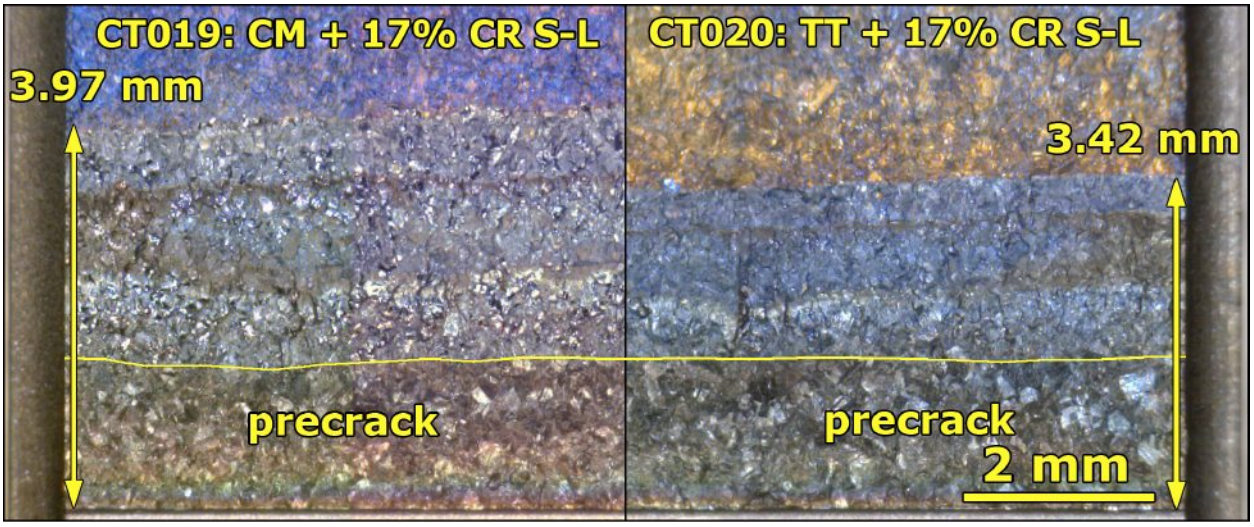

Figure 13. Optical image of crack-growth surface of the 17% CR S-L specimens. Half of each specimen shown in this figure.

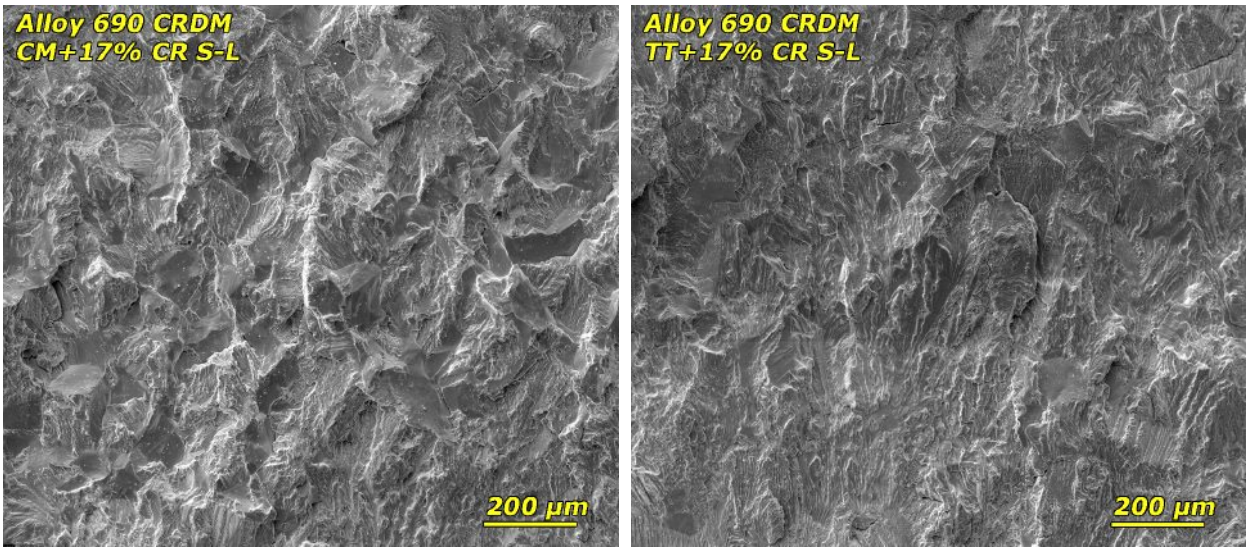

(a) (b)

Figure 14. SEM images of crack-growth surface features in the (a) CM+17% CR S-L and the (b) TT+17% CR S-L specimens.

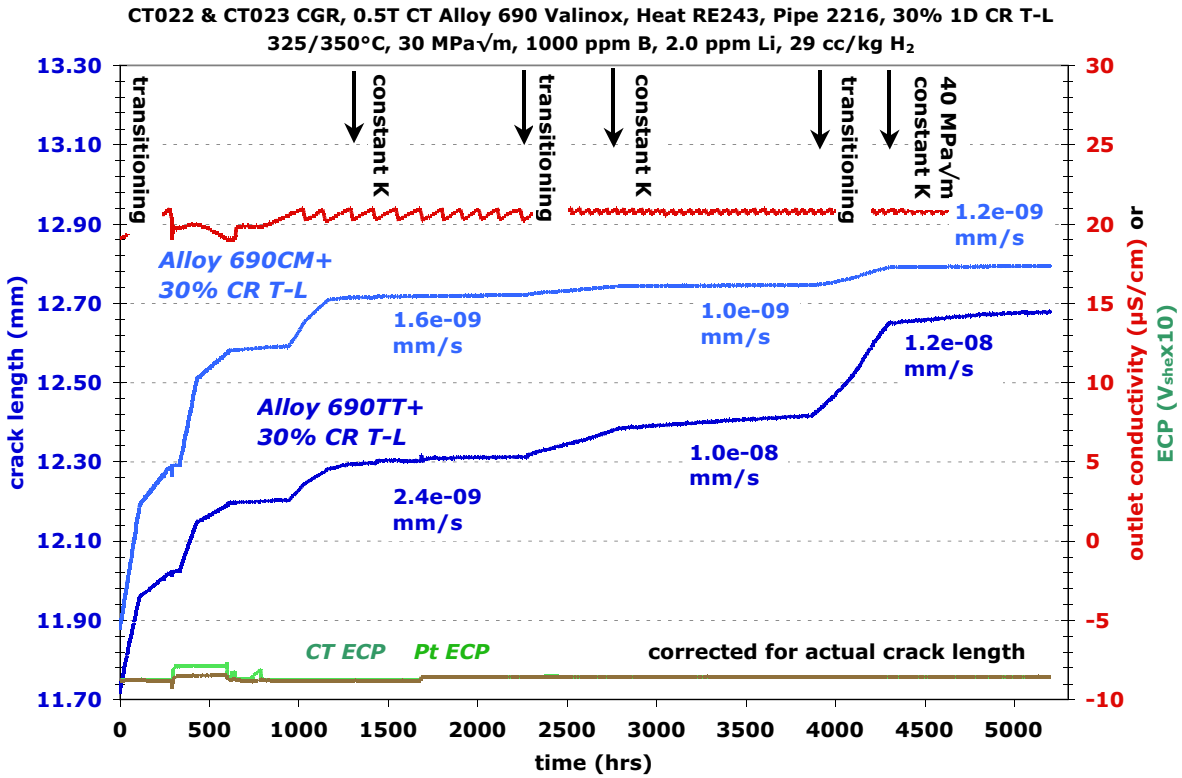

Figure 15. Overview of the crack growth response of the alloy 690TT and CM 30% CR T-L specimens tested at 325°C and 350°C.

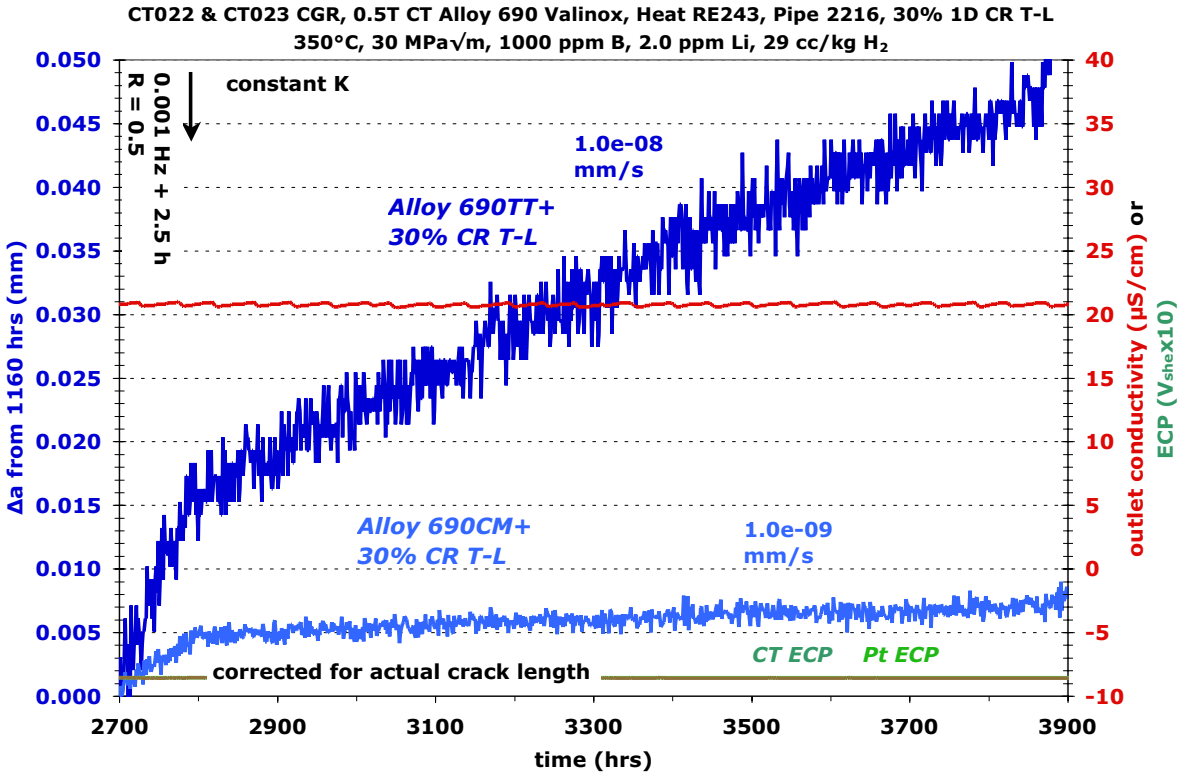

Figure 16. Crack growth response of the alloy 690TT and CM 30% CR T-L specimens during the second assessment of constant K crack growth.

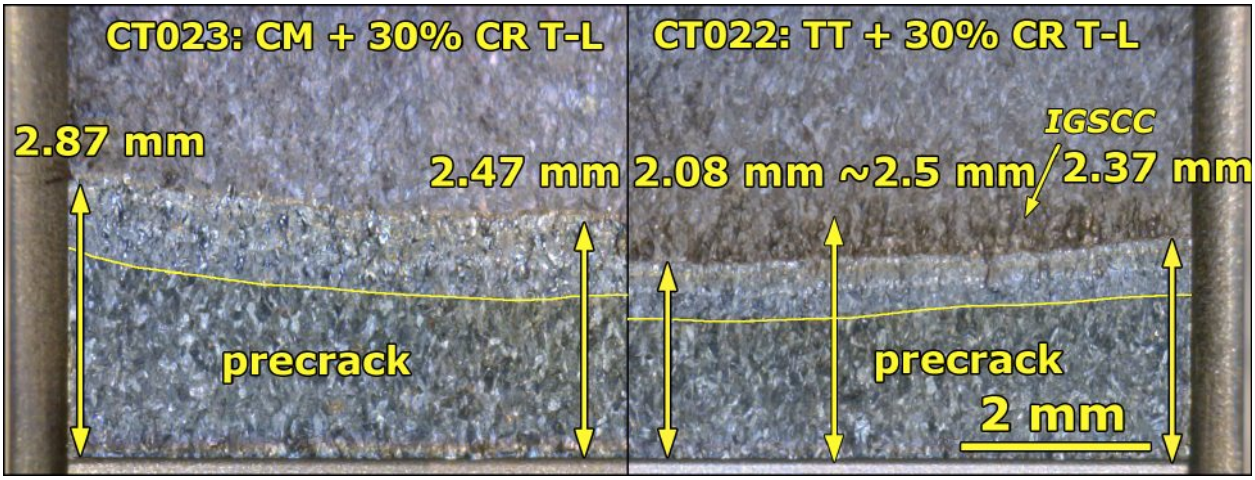

Figure 17. Optical image of the crack-growth surface of the 30% CR T-L specimens. As with the 17% CR T-L specimens, the CM specimen exhibits a greater amount of crack extension during load cycling.

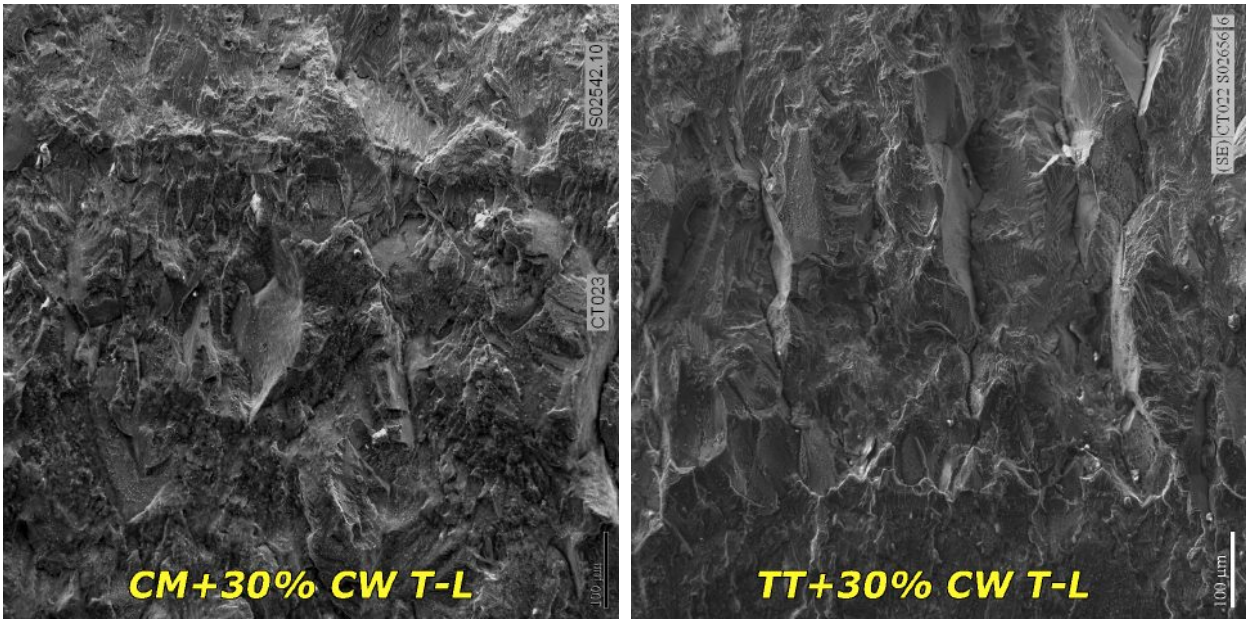

(a) (b)

Figure 18. SEM images of crack-growth surfaces for the 30% CR T-L specimens. Intergranular cracking is observed in both specimens, but with more IG cracking in the TT specimen. Note that IG cracking is on grain boundaries parallel to the rolling plane (transverse plane).

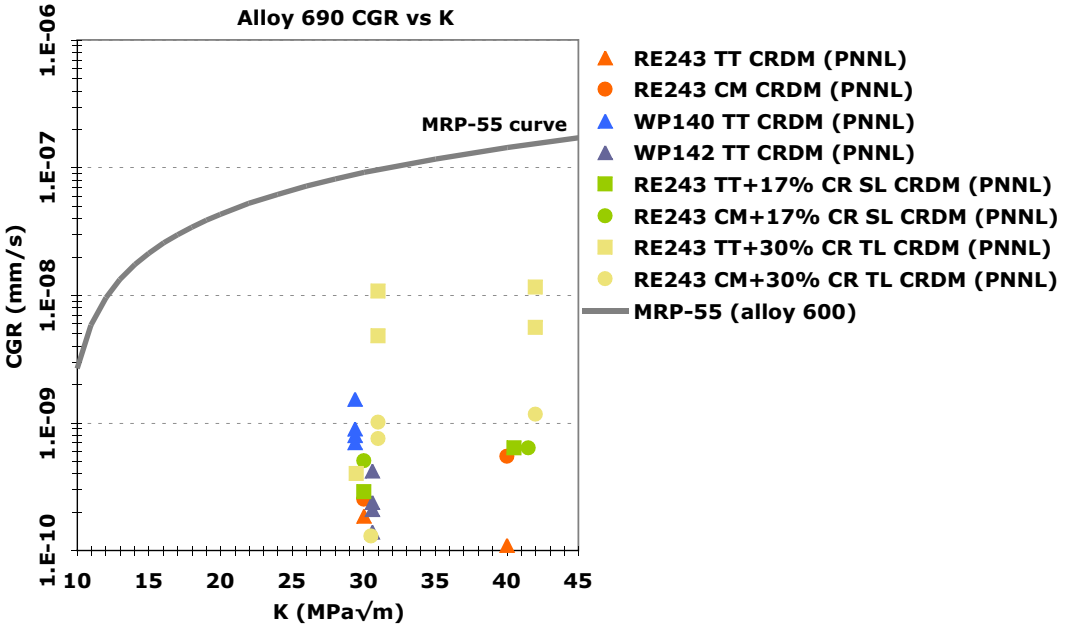

Figure 19. Summary of constant K crack-growth-rate data from tests performed at PNNL on alloy 690 CRDM materials.

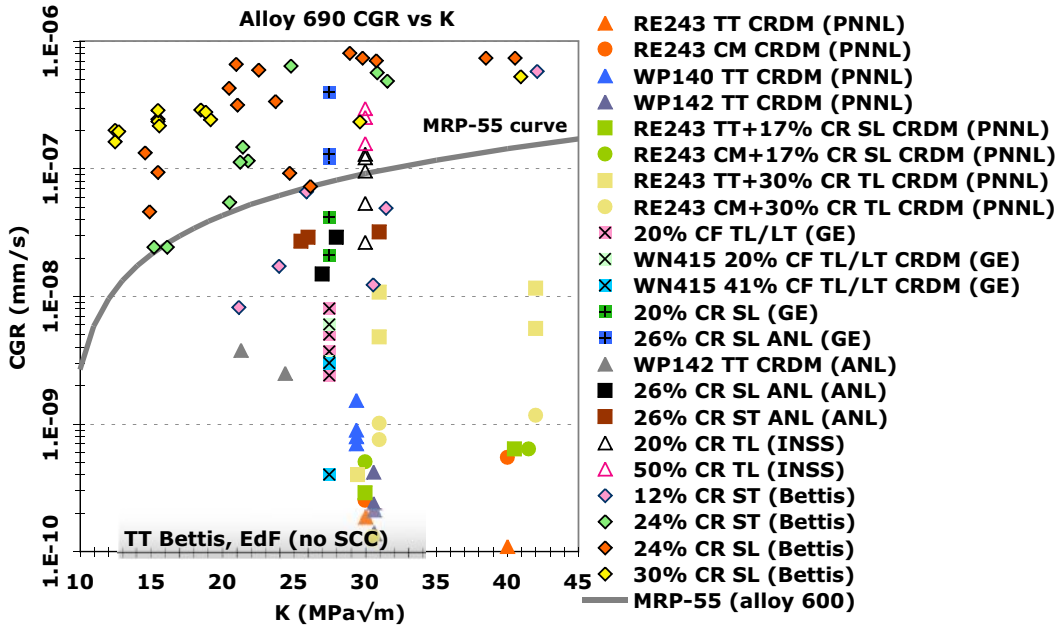

Figure 20. PNNL alloy 690 crack-growth-rate data plotted in comparison to selected alloy 690 crack-growth rate data from GE [6], ANL [8,10], INSS [11], and Bettis [5].